Critical Temperature of a Trapped, Weakly Interacting Bose Gas

F. Gerbier,* J. H. Thywissen,† S. Richard, M. Hugbart, P. Bouyer, and A. Aspect

*Groupe d'Optique Atomique, Laboratoire Charles Fabry de l'Institut d'Optique,
UMR 8501 du CNRS, 91403 Orsay CEDEX, France*

We report on measurements of the critical temperature of a harmonically trapped, weakly interacting Bose gas as a function of atom number. Our results exclude ideal-gas behavior by more than two standard deviations, and agree quantitatively with mean-field theory. At our level of sensitivity, we find no additional shift due to critical fluctuations. In the course of this measurement, the onset of hydrodynamic expansion in the thermal component has been observed. Our thermometry method takes this feature into account.

Degenerate atomic Bose gases provide an ideal testing ground for the theory of quantum fluids. First, their diluteness makes possible first-principles theoretical approaches [1]. Second, thanks to the powerful experimental techniques of atomic physics, static and dynamic properties can be studied quantitatively through a wide range of temperature and densities. Furthermore, the inhomogeneity induced by the external trapping potential leads to entirely new behavior, when compared to bulk quantum fluids.

Atomic interactions have previously been found to affect deeply the dynamical behavior of trapped Bose gases at finite temperatures [2,3]. By contrast, the influence of interactions on *thermodynamics* is less pronounced [4], and has been less studied experimentally. Pioneering work on thermodynamics [5] concentrated essentially on the ground state occupation, and the role of interactions was somewhat hidden by finite-size effects [1]. Though several such measurements have been reported [3,6], to our knowledge a decisive test of the role of interactions is still lacking.

In this Letter, we focus on the critical temperature T_c of a harmonically trapped ^{87}Rb Bose gas to demonstrate the influence of interactions on the thermodynamics. We study the behavior of T_c as a function of the number of atoms at the transition, for a fixed trapping geometry. We find a deviation from ideal-gas behavior, towards lower critical temperatures, whose significance will be discussed below. In the course of this study, we have observed that collisions induce an anisotropy in the free expansion of the cloud even far from the hydrodynamic regime [7,8]. We correct for this effect in our temperature measurement.

For an ideal Bose gas in a harmonic trap, the critical temperature is [1]

$$k_B T_c^{ideal} \approx \hbar\overline{\omega}\left[\frac{N}{\zeta(3)}\right]^{1/3} - \frac{\zeta(2)}{6\zeta(3)}\hbar(\omega_z + 2\omega_\perp). \quad (1)$$

The first term on the right-hand side is the transition temperature T_c^0 in the thermodynamic limit, and the second represents finite-size corrections. Here N is the total atom number, $\omega_\perp$ and ω_z are the trapping frequencies, $\overline{\omega} = \omega_\perp^{2/3}\omega_z^{1/3}$ is their geometrical average, and ζ is the Riemann zeta function.

As stated earlier, the main goal of this paper is to probe the role of two-body repulsive interactions on T_c. Corrections to the ideal-gas formula depend on the ratio between the *s*-wave scattering length a and $\lambda_0 = (2\pi\hbar^2/Mk_B T_c^0)^{1/2}$, the de Broglie wavelength at the transition. In a trapped gas, the dominant effect of interactions can be understood using a simple mean-field picture [4]: Interactions lower the density in the center of the trap $n(0)$, and accordingly decrease the temperature that meets Einstein's criterion $n(0)\lambda_0^3 = \zeta(3/2)$. The magnitude of this reduction has been calculated to leading order [4],

$$\frac{T_c - T_c^{ideal}}{T_c^0} = -a_1\frac{a}{\lambda_0} \approx -1.326\frac{a}{\overline{\sigma}}N^{1/6}, \quad (2)$$

where $a_1 \approx 3.426$ [4,9], and $\overline{\sigma} = \sqrt{\hbar/M\overline{\omega}}$ is the mean ground state width. In this work, the finite-size correction in Eq. (1) changes T_c^0 by at most 2%, whereas the interactive shift (2) can be as high as 10%. The measurements presented below are in quantitative agreement with the prediction of Eq. (2).

As discussed in [9–14], critical fluctuations that develop in the system near T_c are expected to favor the formation of the condensate and thus to increase T_c. In the case of a uniform Bose gas [12–14], this is the leading effect, because the critical temperature is not affected at the mean-field level. The correction $\delta T_c/T_c^0 = +c_1 a/\lambda_0$, with $c_1 \approx 1.3$ [14], can be traced back to density fluctuations with a wavelength much larger than the correlation radius $r_c \sim \lambda_0^2/a$ [13]. This upwards trend, which has been observed experimentally in a dilute sample of ^{4}He adsorbed in a porous glass [15], is quite sensitive to the presence of an external potential [9,11]. In the trapped case of interest here, the contribution of long wavelength excitations to the shift in T_c scales as a higher power of a/λ_0, making it negligible when compared to the "compressional" shift given by Eq. (2). The quantitative

agreement we find with the mean-field result can be considered evidence of this effect, and highlights the important role played by the trapping potential.

Our experimental setup to reach Bose-Einstein condensation in the $|F = 1; m_F = -1\rangle$ hyperfine ground state of ^{87}Rb is similar to that used in [16]. The trapping frequencies are $\omega_\perp/2\pi = 413(5)$ Hz and $\omega_z/2\pi = 8.69(2)$ Hz in the present work. To reduce nonequilibrium shape oscillations that occur in such anisotropic traps upon condensation [8,16], the last part of the evaporation ramp is considerably slowed down (to a ramp speed of 200 kHz/s) and followed by a 1 s hold time in the presence of a radiofrequency shield. We ensure good reproducibility of the evaporation ramp in the following way. We monitor regularly (typically every four cycles) the radiofrequency ν_0 that empties the trap. This allows us to detect slow drifts of the trap bottom, and to adjust in real time the final evaporation radiofrequency ν_{rf} to follow them. In this way, the "trap depth" $\nu_{rf} - \nu_0$, is kept constant within ± 2 kHz. Since we measure $\eta = h(\nu_{rf} - \nu_0)/k_B T \approx 11$ in this final evaporation stage, we estimate the temperature stability to be ± 10 nK.

We infer the properties of the clouds by absorption imaging. After rapid switchoff of the trap ($1/e$ cutoff time of about 50 μs), a 22.3 ms free expansion, and a repumping pulse, we probe the ultracold cloud on resonance with the $|F = 2\rangle \rightarrow |F' = 3\rangle$ transition [17]. The images are analyzed using a standard procedure, described, for instance, in [18]. For an ideal thermal cloud above the transition point, the evolution of the density in time of flight is related to the initial density profile by simple scaling relations, so that the column density (integrated along the probe line of sight, almost perpendicular to the long axis of the trap) is

$$\tilde{n}_{th}(\boldsymbol{\rho}) = \tilde{n}_{th}(0)g_2\left\{\exp\left(\frac{\mu}{k_B T} - \frac{x^2}{2R_{th}^2} - \frac{z^2}{2L_{th}^2}\right)\right\}, \quad (3)$$

where $g_2(u) = \sum_{j\geq 1} u^j/j^2$, and x and z are the coordinates along the tight and shallow trapping axes, respectively. For mixed clouds containing a normal and a (small) Thomas-Fermi (TF) condensate [1], we describe the bimodal distribution by an inverted parabola on top of an ideal, quantum-saturated thermal distribution [Eq. (3) with $\mu = 0$]. The condensed number N_0 is then deduced from the TF fit, and the total atom number N from integration over the entire image. We estimate that condensed fractions as low as 1% can be reliably detected by the fitting routine. Absolute accuracy on atom number relies on the precise knowledge of the absorption cross section of the probe laser, which depends on its polarization and the local magnetic field. This cross section is calibrated by fitting the radial sizes of condensates with no discernible thermal fraction to the TF law $R_0 \propto N_0^{1/5}$ [1,7,18,19]. We find a reduction of 4.00(14) compared to the reference value $\sigma_0 = 3\lambda_L^2/2\pi$ [17].

We will now discuss the more complex issue of thermometry in some detail. The temperature is usually inferred from the sizes of the thermal cloud after a time of flight t, assuming a purely ballistic expansion with isotropic mean velocity, $v_0 = \sqrt{k_B T/M}$, as appropriate for an ideal gas. We show in Fig. 1 that the observed aspect ratio of noncondensed clouds, in a wide range of temperatures and atom numbers (corresponding to $1 \lesssim T/T_c \lesssim 1.8$), is actually larger than the value (0.773) expected for an ideal gas and $\omega_z t \approx 1.23$ that corresponds to our parameters (dotted line in Fig. 1), in contradiction with the assumption of an isotropic velocity distribution.

In a very elongated trap, this could be explained by two distinct collisional effects. First, the initial mean-field energy of the nondegenerate cloud converts almost completely into *radial* kinetic energy during time of fight [20], as for an elongated condensate [7,19]. The magnitude of this effect is controlled by the ratio χ of the mean-field energy to the temperature. In our case, the parameter χ does not exceed 0.02, too low to explain the observed anisotropy (dashed line in Fig. 1, calculated along the lines of [20]).

Second, as studied theoretically in [7,21,22] and observed in Bose [8] and Fermi gases [23], anisotropic expansion occurs for a cloud in the hydrodynamic regime, i.e., when the mean-free path at equilibrium is smaller than the dimensions of the sample. In our very elongated cloud, the mean-free path is typically smaller than the axial length, but much larger than the radial size. Hydrodynamic axial motion of the thermal particles results in energy transfer from the axial to the radial degrees of freedom. For weak deviations from ballistic expansion, this collisional dynamic creates a velocity imbalance proportional to γ_{coll}, the equilibrium collision rate, in agreement with the trend observed in Fig. 1.

In [22], a set of scaling equations was derived to investigate how collisions affect the expansion of a noncondensed cloud. Numerical solution of these equations, which also include the weak mean-field effect, agrees well with our data (solid line in Fig. 1). The calculation
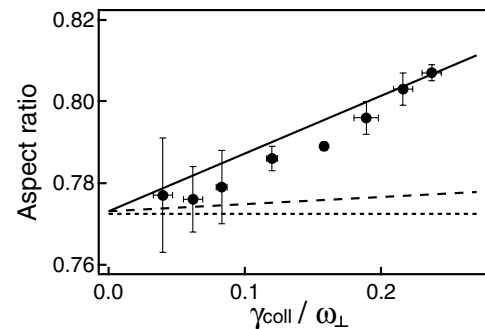

FIG. 1. Onset of hydrodynamic expansion for trapped clouds above threshold. Measured aspect ratios after expansion (filled circles, with statistical error bars) are plotted versus the collision rate γ_{coll}, and compared against several hypotheses: a ballistic expansion (dotted line); a mean field dominated expansion (dashed line); and a collisional expansion for a noncondensed Bose gas (solid line).

makes use of the results of [24] for the collision rate of a noncondensed, almost ideal Bose gas, in general larger (by as much as 70% close to T_c) than the classical collision rate with the same N and T [25]. In view of the satisfactory agreement of our data with the scaling theory, we conclude that the observed anisotropy is a signature of the onset of hydrodynamic expansion.

In the regime $\gamma_{\mathrm{coll}} \lesssim \omega_\perp$, where the anisotropy is weak and increases linearly with γ_{coll}, kinetic energy conservation suggests that mean square expansion velocities take the form $\langle v_x^2 \rangle / v_0^2 \approx 1 + \beta \gamma_{\mathrm{coll}} / 2\omega_\perp$, and $\langle v_z^2 \rangle / v_0^2 \approx 1 - \beta \gamma_{\mathrm{coll}} / \omega_\perp$, where β depends in general on $\omega_\perp, \omega_z, t$ (fixed for the measurement presented here). These simple forms are confirmed by the numerical calculation described above. Provided the expansion velocities along both axes are measured, they allow to infer the initial temperature T_0, independently of the coefficient β [26]. Were this correction not applied, a systematic 10%–15% discrepancy between the axial and radial temperature would remain. We estimate the remaining systematic uncertainties on T as $\pm 5\%$ [27].

Having identified an appropriate thermometric technique, we turn to the measurement of the critical temperature as a function of atom number. Data were taken in a narrow range around T_c. From the two-component fit, we extract the number of condensed atoms, the temperature, and the total atom number as a function of the trap depth, as shown in Figs. 2(a)–2(c), respectively. The trap depth at which the transition point is reached, $(\nu_{\mathrm{rf}} - \nu_0)_c$, is taken to be the point at which a linear fit to the condensed number data crosses zero (a linear approach towards T_c is consistent with the simulations reported in [28]). The temperature and total number are also fitted assuming a linear dependency on ν_{rf}, and from the value $(\nu_{\mathrm{rf}} - \nu_0)_c$ we extract the critical atom number N_c and critical temperature T_c.

In Fig. 3, we plot T_c as a function of N_c, measured in ten independent data sets. The ideal-gas value T_c^{ideal}

(dashed line) lies two standard deviations above our data. Including the mean-field correction (2) yields a much better agreement (solid line), which we quantify by assuming that the interactive shift in T_c can be written as $\delta T_c / T_c^0 = \alpha N^{1/6}$, with a free coefficient α. A fit to the data yields $\alpha = -0.009(1)^{+0.002}_{-0.001}$, whereas Eq. (2) predicts $\alpha \approx -0.007$ for a scattering length $a \approx 5.31$ nm [29] and $\bar{\sigma} \approx 1.00 \ \mu m$. The first uncertainty is statistical, while the upper and lower bounds reflect calibration and analysis uncertainties. The shaded area in Fig. 3 delineates the resulting 1σ confidence interval compatible with the experimental results.

The data shown in Fig. 3 reasonably exclude any additional shift of the same order of magnitude as the compressional effect given by Eq. (2). In particular, if the (positive) critical shift in T_c predicted in the uniform case [12] were directly scalable to the trapped one, one would expect an overall $\alpha \approx -0.004$, a value not consistent with our findings within the estimated accuracy. This observation is in line with recent theoretical studies [9,11], which point out that, instead of being delocalized over the entire system as in the homogeneous case, critical fluctuations in the trapped gas are confined to a small region around the trap center. This reduces corrections to the equation of state by a factor $\sim (a/\lambda_0)^3 \ll 1$, corresponding to the ratio of the volume of the fluctuation region to the volume of the thermal cloud. Corrections to the critical temperature are thus fixed by the equation of state of the whole interacting cloud, and deviations from mean-field behavior enter only to second order in a/λ_0 [30]. For our experimental parameters, we calculate from [9] an upwards correction to T_c smaller than 1%, below the sensitivity of the measurement.

In summary, we have measured the critical temperature of a trapped, weakly interacting ^{87}Rb Bose-Einstein gas. Our results exclude ideal-gas behavior by two standard deviations, and we find satisfactory agreement with
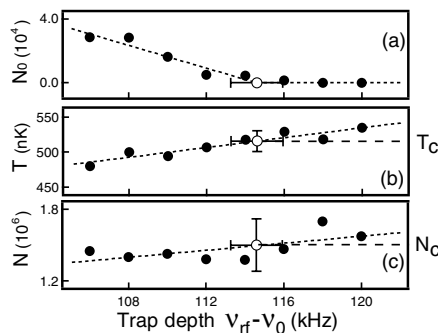

FIG. 2. Procedure to locate the transition point. We plot the condensed number (a), temperature (b), and total atom number (c) as a function of the trap depth, fixed by the final rf frequency ν_{rf} and the trap bottom ν_0. The transition point (hollow circle, with statistical error bars) is found from a piecewise linear fit [dotted curve in (a)], and reported in (b) and (c) to find T_c and N_c.
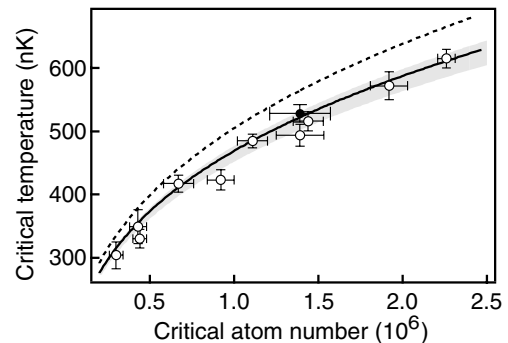

FIG. 3. Critical temperature as a function of atom number at the transition. The experimental points (circles) are lower than the ideal gas law Eq. (1) (dashed) by two standard deviations. The shaded area is the range of acceptable fits taking statistical and systematic errors into account. Our results are consistent with the shift due to the compressional effect given by Eq. (2), indicated by the solid line. The filled circle represents the data of Fig. 2.

mean-field theory. We find no evidence for critical behavior close to T_c within our experimental sensitivity, in line with recent theoretical estimates for the trapped case. We have also observed hydrodynamic behavior in the expansion of the thermal cloud, and shown how to correct for it in the thermometry procedure. We note to conclude that measuring corrections to T_c beyond the mean field for our typical experimental parameters would require thermometry with an accuracy of 1% or better. A more direct route to investigate such effects might be to measure the critical density near the center of the trap, directly sensitive to the presence of critical fluctuations. Alternatively, these many-body effects could be enhanced in the vicinity of a Feshbach resonance.

---

*Electronic address: fabrice.gerbier@iota.u-psud.fr

†Current address: Department of Physics, University of Toronto, Toronto, ON, M5S 1A7, Canada.

[1] F. Dalfovo, S. Giorgini, L. P. Pitaevskii, and S. Stringari, Rev. Mod. Phys. **71**, 463 (1999).

[2] D. S. Jin, M. R. Matthews, J. R. Ensher, C. E. Wieman, and E. A. Cornell, Phys. Rev. Lett. **78**, 764 (2001); D. M. Stamper-Kurn, H.-J. Miesner, S. Inouye, M. R. Andrews, and W. Ketterle, Phys. Rev. Lett. **81**, 500 (1998); F. Chevy, V. Bretin, P. Rosenbusch, K. W. Madison, and J. Dalibard, Phys. Rev. Lett. **88**, 250402 (2002).

[3] O. Maragò, G. Hechenblaikner, E. Hodby, and C. Foot, Phys. Rev. Lett. **86**, 3938 (2001).

[4] S. Giorgini, L. P. Pitaevskii, and S. Stringari, Phys. Rev. A **54**, R4633 (1996); J. Low Temp. Phys. **109**, 309 (1997).

[5] J. R. Ensher, D. S. Jin, M. R. Matthews, C. E. Wieman, and E. A. Cornell, Phys. Rev. Lett. **77**, 4984 (1996).

[6] M.-O. Mewes, M. R. Andrews, N. J. van Druten, D. M. Kurn, D. S. Durfee, and W. Ketterle, Phys. Rev. Lett. **77**, 416 (1996); D. J. Han, R. H. Wynar, Ph. Courteille, and D. J. Heinzen, Phys. Rev. A **57**, R4114 (1998); B. P. Anderson and M. A. Kasevich, Phys. Rev. A **59**, R938 (1999); F. Schreck *et al.*, Phys. Rev. Lett. **87**, 080403 (2001).

[7] Y. Kagan, E. L. Surkov, and G. V. Shlyapnikov, Phys. Rev. A **55**, R18 (1997).

[8] I. Shvarchuck *et al.*, Phys. Rev. Lett. **89**, 270404 (2002).

[9] P. Arnold and B. Tomášik, Phys. Rev. A **64**, 053609 (2001).

[10] M. Houbiers, H. T. C. Stoof, and E. A. Cornell, Phys. Rev. A **56**, 2041 (1997).

[11] M. Holzmann, J.-N. Fuchs, J.-P. Blaizot, G. Baym, and F. Laloë, cond-mat/0310460.

[12] P. Grüter, D. Ceperley, and F. Laloë, Phys. Rev. Lett. **79**, 3549 (1997); M. Holzmann, P. Grüter, and F. Laloë, Eur. Phys. J. B **10**, 739 (1999).

[13] G. Baym, J.-P. Blaizot, M. Holzmann, F. Laloë, and D. Vautherin, Phys. Rev. Lett. **83**, 1703 (1999); G. Baym, J.-P. Blaizot, and J. Zinn-Justin, Europhys. Lett. **49**, 150 (2000); M. Holzmann, G. Baym, J.-P. Blaizot, and F. Laloë, Phys. Rev. Lett. **87**, 120403 (2001).

[14] P. Arnold and G. Moore, Phys. Rev. Lett. **87**, 120401 (2001); V. A. Kashurnikov, N. V. Prokof'ev, and B. V. Svistunov, Phys. Rev. Lett. **87**, 120402 (2001).

[15] J. D. Reppy, B. C. Crooker, B. Hebral, A. D. Corwin, J. He, and G. M. Zassenhaus, Phys. Rev. Lett. **84**, 2060 (2000).

[16] S. Richard, F. Gerbier, J. H. Thywissen, M. Hugbart, P. Bouyer, and A. Aspect, Phys. Rev. Lett. **91**, 010405 (2003).

[17] The probe laser wavelength is $\lambda_L = 780.2$ nm; its intensity is 0.17 mW/cm^2, and the imaging pulse length is 34 μs. The 8 MHz half-width of the absorption line is slightly broader than the natural linewidth (6 MHz), which could explain the small value of the measured cross section.

[18] W. Ketterle, D. S. Durfee, and D. M. Stamper-Kurn, in *Proceedings of the International School of Physics-Enrico Fermi*, edited by M. Inguscio, S. Stringari, and C. E. Wieman (IOS Press, Amsterdam, 1999).

[19] Y. Castin and R. Dum, Phys. Rev. Lett. **77**, 5315 (1996).

[20] C. Menotti, P. Pedri, and S. Stringari, Phys. Rev. Lett. **89**, 250402 (2002).

[21] H. Wu and E. Arimondo, Europhys. Lett. **43**, 141 (1998).

[22] P. Pedri, D. Guéry-Odelin, and S. Stringari, Phys. Rev. A **68**, 043608 (2003).

[23] K. M. O'Hara, S. L. Hemmer, M. E. Gehm, S. R. Granade, and J. E. Thomas, Science **298**, 2179 (2002); C. A. Regal and D. S. Jin, Phys. Rev. Lett. **90**, 230404 (2003); T. Bourdel *et al.*, Phys. Rev. Lett. **91**, 020402 (2003).

[24] G. M. Kavoulakis, C. J. Pethick, and H. Smith, Phys. Rev. A **61**, 053603 (2000).

[25] We have extrapolated the results of [24] by the formula $\gamma_{\text{coll}} \approx \gamma_{\text{class}}(1 + 0.23/t^3 + 0.4/t^4)$, with $t = T/T_c^0$. Following [22], we define the classical collision rate as $\gamma_{\text{class}} = (4\sqrt{2\pi}/5)n_{\text{class}}(0)\sigma_{\text{el}}v_0$, with $\sigma_{\text{el}} = 8\pi a^2$ and $n_{\text{class}}(0) = N\overline{\omega}^3(m/2\pi k_B T)^{3/2}$.

[26] Defining effective temperatures as $k_B T_i = M\omega_i^2 R_i^2(1 + \tau_i^2)^{-1/2}$, where $R_i|_{i=x,z}$ are the measured cloud sizes and $\tau_i = \omega_i t$, we infer the initial temperature T_0 from $T_0 \approx 2\tau_z^2/(1 + 3\tau_z^2)T_x + (1 + \tau_z^2)/(1 + 3\tau_z^2)T_z$. This cancels the hydrodynamic corrections to first order in $\gamma_{\text{coll}}/\omega_\perp$.

[27] This 5% uncertainty on T takes into account length calibration, the released mean-field energy, and the finite fall time of the current producing the magnetic potential. Note that, in a $T_c - N$ plot, the uncertainty on the *shift* in T_c is smaller because of partial error cancellation.

[28] M. Holzmann, W. Krauth, and M. Naraschewski, Phys. Rev. A **59**, 2956 (1999); T. Bergeman, D. L. Feder, N L. Balazs, and B. I. Schneider, Phys. Rev. A **61**, 063605 (2000).

[29] E. G. M. van Kempen, S. Kokkelmans, D. J. Heinzen, and B. J. Verhaar, Phys. Rev. Lett. **88**, 093201 (2002).

[30] These corrections are provided by critical fluctuations with wavelength $\lesssim r_c$, barely affected by the trap potential.